Self-Assembly Mechanism of pH-Responsive Glycolipids: Micelles, Fibers, Vesicles, and Bilayers — Source link ↗

Niki Baccile, Anne-Sophie Cuvier, Sylvain Prévost, Christian V. Stevens ...+6 more authors

Institutions: Collège de France, Ghent University, Bio Base Europe

Topics: Micelle, Vesicle, Oleic acid, Bilayer and Amphiphile

Related papers:

- pH-Driven Self-Assembly of Acidic Microbial Glycolipids

- pH-triggered formation of nanoribbons from yeast-derived glycolipid biosurfactants.

- Unusual, pH-Induced, Self-Assembly Of Sophorolipid Biosurfactants

- Structure of Bolaamphiphile Sophorolipid Micelles Characterized with SAXS, SANS, and MD Simulations

- Micelles versus Ribbons: How Congeners Drive the Self-Assembly of Acidic Sophorolipid Biosurfactants.

Share this paper: 𝟙 🐦 in ✉

View more about this paper here: https://typeset.io/papers/self-assembly-mechanism-of-ph-responsive-glycolipids-se7sj35s8z

Self-Assembly Mechanism of pH-Responsive Glycolipids: Micelles, Fibers, Vesicles, and Bilayers

Niki Baccile,*,[†] Anne-Sophie Cuvier,[†] Sylvain Prévost,[‡] Christian V. Stevens,[§] Elisabeth Delbeke,[§] Jan Berton,[§] Wim Soetaert,[∥] Inge N. A. Van Bogaert,[∥] and Sophie Roelants[∥,⊥]

[†]Sorbonne Universités, UPMC Univ Paris 06, CNRS, Collège de France UMR 7574, Chimie de la Matière Condensée de Paris, UMR 7574, F-75005 Paris, France

[‡]ESRF - The European Synchrotron, High Brilliance Beamline ID02, 38043 Grenoble, France

[§]SynBioC, Department of Sustainable Organic Chemistry and Technology, Ghent University, Ghent, Belgium

[∥]InBio, Department of Biochemical and Microbial Technology, Faculty of Bioscience Engineering, Ghent University, Coupure Links 653, 9000 Ghent, Belgium

[⊥]Bio Base Europe Pilot Plant, Rodenhuizekaai 1, 9042 Ghent, Belgium

Ⓢ *Supporting Information*

ABSTRACT: A set of four structurally related glycolipids are described: two of them have one glucose unit connected to either stearic or oleic acid, and two other ones have a diglucose headgroup (sophorose) similarly connected to either stearic or oleic acid. The self-assembly properties of these compounds, poorly known, are important to know due to their use in various fields of application from cleaning to cosmetics to medical. At basic pH, they all form mainly small micellar aggregates. At acidic pH, the oleic and stearic derivatives of the monoglucose form, respectively, vesicles and bilayer, while the same derivatives of the sophorose headgroup form micelles and twisted ribbons. We use pH-resolved *in situ* small angle X-ray scattering (SAXS) under synchrotron radiation to characterize the pH-dependent mechanism of evolution from micelles to the more complex aggregates at acidic pH. By pointing out the importance of the $COO^-/COOH$ ratio, the melting temperature, T_m, of the lipid moieties, hydration of the glycosidic headgroup, the packing parameter, membrane rigidity, and edge stabilization, we are now able to draw a precise picture of the full self-assembly mechanism. This work is a didactical illustration of the complexity of the self-assembly process of a stimuli-responsive amphiphile during which many concomitant parameters play a key role at different stages of the process.
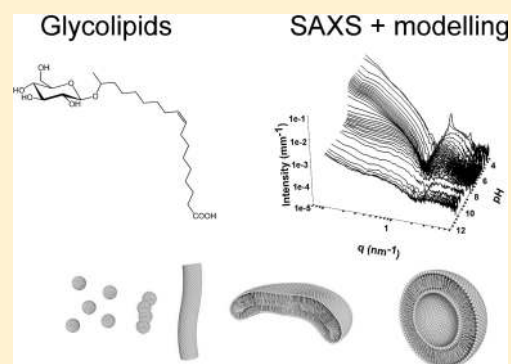
INTRODUCTION

Stimuli-responsive self-assembly is an active field of research in the domain of soft matter due to the broad number of potential applications.[1] Block copolymers and lipids are commonly designed to tune their self-assembly properties in solution as a function of temperature (e.g., use of *N*-isopropylacrylamide residues), pH (use of amine or carboxylic acid residues), ionic force (use of charged residues), etc.[2] Typical self-assembled structures range, for example, from simple spherical to branched micelles, disks, vesicles, sheets, and fibers,[1,3−5] and the morphological relationship between them is generally considered to rely on the molecular structure, according to the well-known packing parameter relationship.[6] Cone-like molecular morphologies tend to form curved objects, like micelles, while cylinder-shaped molecules rather form bilayers. Although this simplistic view can explain or even predict the shape of the micellar aggregates for various amphiphilic systems on a thermodynamic basis (e.g., ethylene oxide, ionic, gemini surfactants, ...),[7−10] it fails to describe many experimental facts, as this is well-known among physico-chemists.[11] Other

factors, often concomitant, play crucial roles in determining the structure−property relationship in soft systems. Typical factors influencing the self-assembly properties of lipids and block copolymers are the presence of Coulomb attraction/repulsion forces, the nature of counterions, temperature, hydration, rigidity of the aliphatic chain, entropy gain/loss, kinetics, steric repulsion, chirality, H-bonding, mechanical, etc. The following examples of surfactants illustrate this point: gemini surfactants, and in particular quaternary ammonium-based ones, are known to form micelles in water.[12] However, in the presence of an organic acid as a counterion, they can form helical/twisted fibers.[13] Fatty acid salts are known to form micelles under basic pH conditions, whereas they become immiscible in their acidic form. However, in a narrow pH range between 7 and 9, they are able to form vesicular objects under accurate control of the starting conditions and the $COO^-/COOH$ ratio.[5] Phospholi-

pids, the major constituent of the cell membrane, generally form planar bilayers. However, upon change of the water osmotic pressure or upon introduction of a cosurfactant (bile salts are often described in the literature), the bilayer membrane curvature can be modified.[14] Vesicles, interesting objects for their encapsulation properties which are often used in drug delivery applications,[1] are commonly obtained through mechanical treatment (shear force, filtration, sonication) of lamellar phospholipid phases.[15] The examples above show the high degree of complexity in the fundamental understanding of amphiphilic systems and, above all, in the beforehand prediction of the most stable final structure. A further example is provided by the self-assembly properties of peptide nanotubes, for which the mechanism of formation was reported to depend on the way they are prepared, either by dispersion of the peptide in water at room temperature (dissolution reassembly mechanism) or by a heating–cooling step (oriented attachment).[16] If, in this specific case, the process is believed to depend on the different supersaturation level of the peptide in solution, the importance of kinetics in self-assembly has also been emphasized in the past decade, as largely described by Leng et al.;[17] for instance, the rate at which a given stimulus is applied (e.g., slow variation in temperature or in pH induces the formation of large, or more aggregated, vesicles in tetraethylene glycol-based or phospholipid amphiphiles) is known to have a potential effect.[18,19] If an exhaustive list of examples is practically impossible, the main message is that it is impossible nowadays to predict the self-assembly properties in solution of a given compound on the sole basis of its molecular structure.

In this work, we present four microbial sugar-based bolaamphiphiles, of which the chemical structures are closely related and of which the self-assembly behavior could be expected to be similar. Two structurally similar sophorolipid molecules have been selected, both containing a glucose $\beta(1,2)$ disaccharide (sophorose) as the hydrophilic head, but a different C18 fatty acid tail, namely, oleic acid for the SL-C18:1 (monounsaturation in position 9,10) compound and stearic acid for the SL-C18:0 (fully saturated), as shown in Figure 1. The second set of compounds has exactly the same fatty acid tails but a single β-D-glucose hydrophilic headgroup, instead of the disaccharide (G-C18:1 and G-C18:0 compounds, Figure 1).

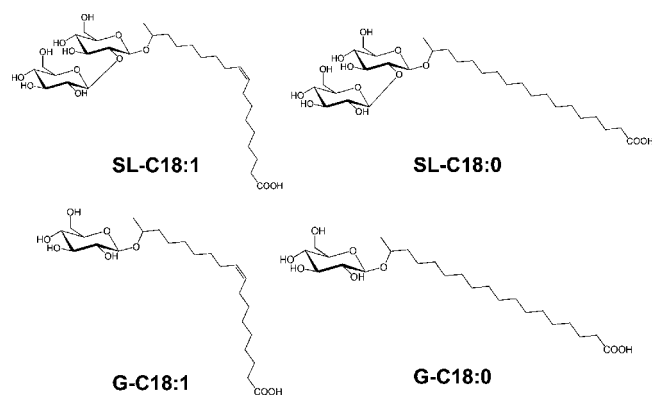Sugar-based amphiphiles are a class of molecules which attract much attention due to their biobased origin combined with their astonishing self-assembly properties in water.[20−25] The broad variety of supramolecular structures (micelles, vesicles, fibers, bilayers, chiral fibers)[26−28] they can form makes them valuable substitutes for synthetic, more classical families of amphiphiles, like alkylammonium and alkylsulfate salts or block copolymers, yet these sugar-based amphiphiles exhibit a rich self-assembly behavior. Given the importance of carbohydrates in glycobiology and medicine,[29,30] and the richness of carbohydrate chemistry, the applications of glycolipids are potentially broader than those for engineered amphiphiles.[31] In addition, the biobased microbial origin of the glycolipids selected for this study makes them interesting alternative candidates to both petroleum-based compounds. Microbial glycolipids, also known as "biosurfactants", have a good biodegradability, low cytotoxicity, and numerous applications as antimicrobial, antibiofilm, anticancer, emulsifying, and stabilizing agents already exist.[32−34] Scaled-up production is nowadays possible, as various companies (e.g., Evonik, Intobio, Jeneil, Soliance) have an ongoing biosurfactants (sophorolipids in particular) production. If counter arguments against biosurfactants state that the cost is still high due to limited production and purification processes, in the long run, this field is expected to grow more and more, as shown by the new opportunities offered by the selection of genetically modified strains[35] to increase both productivity and selectivity.

The glycolipids selected for this work are characterized by two well-known chemical groups (glucose, fatty acid) which allow direct comparison with more common amphiphiles (phospholipids, anionic and neutral surfactants, fatty acid salts, alkyl polyglycosides, just to cite some). However, their bolaform structure, the unusual behavior of sugars (e.g., via oriented hydrogen bonding[36,37]), and pH-responsive properties are factors which unpredictably influence the self-assembly. At basic pH, all selected compounds form micelles as a major component, although the presence of additional aggregates (platelets, bilayers, ill-defined structures) must also be outlined.[38,39] At acidic pH, SL-C18:1 and SL:C18:0 sophorolipids respectively assemble into micelles[40,41] and twisted ribbons;[42] in addition, G-C18:1 glucolipids form vesicles while G-C18:0 forms infinite bilayer sheets.[39] The aim of this study is to find insights into the structure−property relationships and pH-driven assembly mechanism for a set of structurally related microbial glycolipids using pH-resolved *in situ* small angle X-ray scattering (SAXS). In particular, we will show the tight relationship between the COOH/COO⁻ ratio, the carbohydrate hydration, the lipid melting temperature, T_m, membrane flexibility, and the domain of stability for micelles, ribbons, vesicles, and bilayers.

■ MATERIALS AND METHODS

Microbial glycolipids are known to be a mixture of similar congeners, of which one form is generally the majority (>85%). Figure 1 shows the chemical structures of the most abundant forms of sophorolipids SL-C18:1 and SL-C18:0 and glucolipids G-C18:1 and G-C18:0. SL-C18:1 is obtained from the yeast *Starmerella bombicola*; its synthesis was described elsewhere,[41] and the relative HPLC-ELSD data and composition are given in Figure S1. SL-C18:0 is obtained from the monounsaturated SL-C18:1 by a chemical modification step.[42] Glucolipid G-C18:1 has been obtained using a modified strain (ΔugtB1) of the yeast *S. bombicola*, while G-C18:0 is derived from G-C18:1 through hydrogenation. Sophorolipids are characterized by a glucose $\beta(1,2)$ disaccharide hydrophilic headgroup, while glucolipids contain a single β-D-glucose hydrophilic headgroup. The synthesis

Figure 1. Chemical structures of SL-C18:1 and SL-C18:0 sophorolipids and G-C18:1 and G-C18:0 glucolipids.

Table 1. Main Components of the Sophorolipid (SL-) and Glucolipid (G-) Compounds Used in This Study[a]

	congener					references	
sample	C18:1, subterminal	C18:1, terminal	C18:2, subterminal	C18:0, subterminal	C18:0, terminal	analysis by HPLC-ELSD	former studies
SL-C18:1	86.0	6.0	1.0	1.0	0	this work	38, 41
SL-C18:0	0	0	0	90	10	42	38, 42, 43
G-C18:1	89.6	7.3	1.3	1.8	0	39	39
G-C18:0	0	0	0	92.7	7.3	39	39

[a]C18:2, C18:1, and C18:0 refer to the number of carbons (C18) in the fatty acid chain and number of unsaturations (2, 1, or 0). Subterminal (C17) and terminal (C18) refer to the position of the glycosidic bond in the fatty acid tail with respect to the COOH group (C1). The percentages refer to values estimated by measuring the peak area ratio in HPLC-ELSD measurements. Residual congeners in the SL-C18:1 sample batch are given in the Supporting Information (Figure S1). References indicate previous studies in which these same sample batches have been employed.

procedure and analysis of glucolipids is provided in ref 39. All C18:1 compounds contain a monounsaturation at position C9,10 of the fatty acid, while C18:0 compounds are characterized by a fully saturated chain.

Table 1 gives the exact composition of each sample used in this work determined by the peak area ratio in HPLC-ELSD measurements[42,39] as well as the previous studies in which these same batches have been used. Upon use, all compounds are in their acidic (COOH) form and fully deacetylated. The most abundant species (close to 90% on average) is composed by the glycolipid having the glycosidic bond in the subterminal, C17, position, as indicated in Figure 1. However, unavoidable amounts of congeners are always present, a common fact for all studies on biobased amphiphiles. The largest impurity common to all glycolipids is the terminal, C18, congener of each lipid and which systematically represents between 6 and 10% of the mixture for all compounds.

Sample Preparation. A given amount of the desired compound is dissolved into Milli-Q-grade water at room temperature to give a concentration of 5 mg/mL. The pH is increased up to ∼11.6 by adding 10−15 μL of a 5 M NaOH solution, and it is eventually decreased by adding μL amounts of 0.1 M HCl. This procedure, necessary to solubilize the samples, generates NaCl. However, this is only a minor drawback because all systems are prepared in the same way and, consequently, comparable one to the other. In addition, it was shown that the effect of NaCl in these systems only influences aggregation: NaCl only affects the aspect ratio of SL-C18:1 micelles,[41] while it impacts fiber aggregation, but not their chirality, on SL-C18:0 sophorolipids.[43] Additional arguments supporting the low impact of NaCl will be discussed in the text.

pH-Resolved *in situ* Small Angle X-ray Scattering (SAXS). SAXS experiments have been done using a flow-through polycarbonate 2 mm capillary connected to the sample-containing solution at pH 11.6 through a peristaltic pump. The pH was controlled *in situ* via a classical KCl pH-meter directly located in the experimental hutch and monitored in real time. pH changes have been obtained by using a 0.1 M HCl solution introduced via a motor-controlled press-syringe. If the continuous flow-through device avoids beam damage, we could only acquire one spectrum at each pH under this particular setup, thus making the statistics more fluctuating than classical *ex situ* experimental conditions. Data have been acquired on the high brilliance ID02 beamline at the ESRF synchrotron (Grenoble, France). (E = 12.46 keV, sample-to-detector distance = 1 m) Error bars were calculated on the basis of the estimated number of photons detected (accounting for the gain and quantum efficiency of the CCD and phosphor layer), assuming Poisson statistics. The noise of the detector was accounted for by comparison of dark images. A CCD camera was used to collect the scattered photons and integrated azimuthally to obtain a typical $I(q)$ spectrum. Contribution of the solvent (water at pH 11.6) and capillary have been measured prior to the experiment and duly subtracted during the data treatment. All data have been corrected for the transmission of the direct beam and scaled to be in absolute scale. The detailed analysis of the SAXS data is presented in the Supporting Information (Figure S2).

Transmission Electron Microscopy (TEM). TEM experiments have been performed on an FEI Tecnai 120 Twin microscope

operating at 120 kV equipped with a Gatan Orius SC1000 CCD numeric camera 4k × 4k. A set of TEM images was recorded on a single copper TEM grid onto which a drop of SL-C18:0 solution at pH 11 and 5 mg/mL has been deposited and locally exposed to a concentrated HCl solution for a few seconds before the drop is dried. This operation allows one single grid to contain all objects formed at different stages of their growth, from the precursor micellar/platelet[38] to the twisted ribbon[42] state. Previous experiments[43] have shown that, for this particular system, conventional TEM observation does not affect the fibrillar structure and morphology; for this reason, we use it here in a qualitative way to observe the intermediates of the twisted ribbon formation.

HPLC-ELSD Analysis. HPLC-ELSD analysis was performed with the Agilent 1260 Infinity equipped with an Agilent Zorbax Eclipse Plus C18 column (4.6 × 100 mm − 3.5 μm) at 40 °C. A flow rate of 1 mL/min was applied, and a gradient of two solvents (A, 0.05% acetic acid; B, acetonitrile) was applied using the following method: 0 min, 95% A and 5% B; 25 min, 5% A and 95% B; 27 min, 5% A and 95% B; 30 min, 95% A and 5% B.

LC-MS Analysis. LC-MS analysis of glucolipids was done on a Shimadzu LC-10-AD HPLC system (Shimadzu Europe GmbH, Germany) connected to a quadrupole mass spectrometer (Waters, Milford, MA). Molecules were identified by their native molecular masses after ESI (electron spray ionization) without collision.

■ RESULTS AND DISCUSSION

Basic pH. The SAXS profiles and corresponding fits above q > 1 nm^{-1} using a core−shell ellipsoid of revolution model for all microbial glycolipid samples at pH 11.0 ± 0.3 are given in Figure 2. As it was observed before,[39] all samples have a similar scattering profile characterized by an intense signal below q < 0.3 nm^{-1} and a signature typical for micellar objects above q > 1 nm^{-1}. Very interestingly, the first oscillation of the form factor above 2 nm^{-1} shows remarkable differences between all samples. From a qualitative point of view, SL-C18:1 and G-C18:1 samples have a similar, rather flat, oscillation, which is, on the contrary, more pronounced for SL-C18:0 and G-C18:0 systems. It is well-known that specific ion binding on the hydrophilic polar headgroup modifies the electron spatial distribution with an obvious influence on the final form factor oscillation;[44,45] however, in this situation, all samples are at pH 11 and therefore they contain a comparable amount of Na$^+$. For these reasons, one must attribute the spectroscopic differences to a specific arrangement of the core−shell−solvent interfaces according to the type of glycolipid employed. To better understand that, we have fitted all curves with the same Core−Shell Ellipsoid of Revolution model (CSERm) form factor (refer to the Supporting Information for more details) and we have proceeded as follows in order to understand which are the crucial parameters that have a direct impact on the form factor oscillation profile.
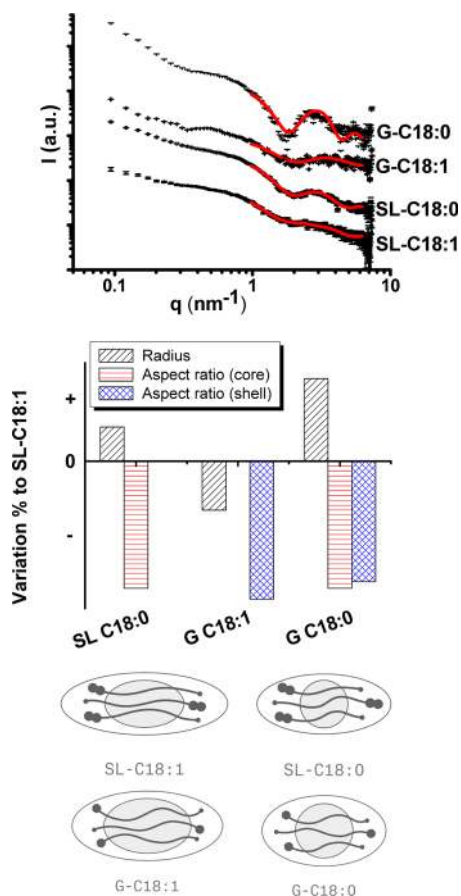
Figure 2. SAXS data (with error bars) corresponding to both sophorolipids and glycolipids (0.5 wt %) at pH 11.0 ± 0.3. The red curves correspond to the fit performed using a core−shell ellipsoid of revolution form factor model. The fitting procedure for this system has been outlined in the Supporting Information. The histogram shows the relative variation of the most significant fitting parameters (radius, aspect ratio (core, shell)), keeping all others constant, for the SL-C18:0, G-C18:1, and G-C18:0 samples and with respect to the reference compound, SL-C18:1. The modeled ellipsoid structures for each glycolipid are given on the bottom of the figure.

First of all, we operate a best fit procedure on the reference SL-C18:1 system, as this was largely studied before both at acidic and basic pH.[41,38] We use the values obtained in ref 38 as starting parameters. The optimized values for this specific system, reported in Table S1, are comparable to those reported in ref 38. We then use this set of values to fit the SL-C18:0 and G-C18:1 profiles, and we vary all parameters one-by-one so as to match the experimental curves at best. We find that the aspect ratio (core) has the strongest impact on the fit of the SL-C18:0 sample, while the radius refines the result. We also find that simultaneous variation of shell SLD and aspect ratio (shell) is necessary to fit the G-C18:1 system, while changes of the radius, R, refine the result. Finally, we use the values found for the SL-C18:0 system to fit the G-C18:0 data and we observe that aspect ratio (shell) and radius only have a minor impact on the quality of the fit. Interestingly, the thickness, T, does not need variation in any of the systems and it was kept constant at 3.93×10^{-1} nm. We must stress the fact that these are not best fits but only adjustments to understand the least number of critical parameters accounting for the spectral differences above $q > 1$ nm^{-1}. For this reason, the absolute values given in Table S1 should be taken with caution; however, the relative variations of the radius, aspect ratio (core), and aspect ratio (shell) in all samples with respect to SL-C18:1 are very informative, as shown in Figure 2.

Given an approximate micellar morphology for the SL-C18:1 sample at pH ∼ 11, depicted in Table S1, one can see that the saturation of the $C_{9,10}$ double bond mainly impacts the micellar core, which becomes practically spherical, while the shell aspect ratio is unchanged (sample SL-C18:0). When keeping the unsaturation but reducing the number of sugar units (sample G-C18:1), the core aspect ratio is unchanged but the shell aspect ratio is reduced, as illustrated in Table S1. Finally, one glucose unit combined with saturation (sample G-C18:0) has a spherical core with a reduced shell aspect ratio.

These data can be generalized as follows: (1) The monounsaturation always drives the formation of an elliptical hydrophobic core, while saturated compounds always have a spherical core. (2) The higher the number of sugar units, the larger the shell size in the axial direction, at constant shell thickness in the equatorial direction. If the second observation is in agreement with the larger size of the sophorose headgroup if compared to glucose, both observations taken together could only be explained by the fact that in all samples the carbohydrate headgroups are mainly located in the axial direction of the shell while the carboxylate groups are probably located in both axial and equatorial directions of the shell. Meanwhile, all saturated (C18:0) compounds seem to form a homogeneous spherical core, while monounsaturated ones (C18:1) tend to be in an ellipsoidal volume, the difference between them probably originating from a combination between electrostatic repulsions of the carboxylate groups and differences in the rigidity of the aliphatic chain at room temperature. In all cases, the core size below 1 nm is in agreement with previous studies[41] on sophorolipids, suggesting interpenetration and bending phenomena of the aliphatic chain, as predicted by Nagarajan[46] on bolaform amphiphiles. Nevertheless, we are never able to describe the system with a homogeneous hydrophilic shell, a fact which, even if it was proposed by Nagarajan,[46] was demonstrated not to be true in the case of SL-C18:1 sophorolipid micelles at pH below 7.41.

pH-Resolved Morphology Transitions. Addition of HCl to the systems described just above drives important morphological changes below a critical pH value, characteristic for each glycolipid.[39] Turbidity experiments have shown that pH values of 7.4, 6.2, and 7.8 mark the transition for, respectively, SL-C18:0, G-C18:1, and G-C18:0 into twisted ribbons, vesicles, and infinite bilayer sheets.[39,42] As for SL-C18:1, no transition pH could be defined on the basis of light scattering experiments.[42] The corresponding pH-dependent *in situ* SAXS experiments on all samples are shown in Figure 3, while the corresponding contour plots are presented in Figure S3. From a qualitative point of view, one can see that all systems present a continuous spectral evolution from basic to acidic pH and that the spectral signature is unchanged from pH ∼ 12 to pH ∼ 8. More specifically:

(a) The broad signal above $q > 1$ nm^{-1} for the SL-C18:1 system (Figure 3) becomes more visible at lower pH, thus putting in evidence a clear rearrangement of the electron density distribution in the micelle, the characteristic signal of which[41] also becomes evident in the low-q region below $q < 1$ nm^{-1}. The SL-C18:1 contour plot in Figure S3 shows the appearance of the first minimum of
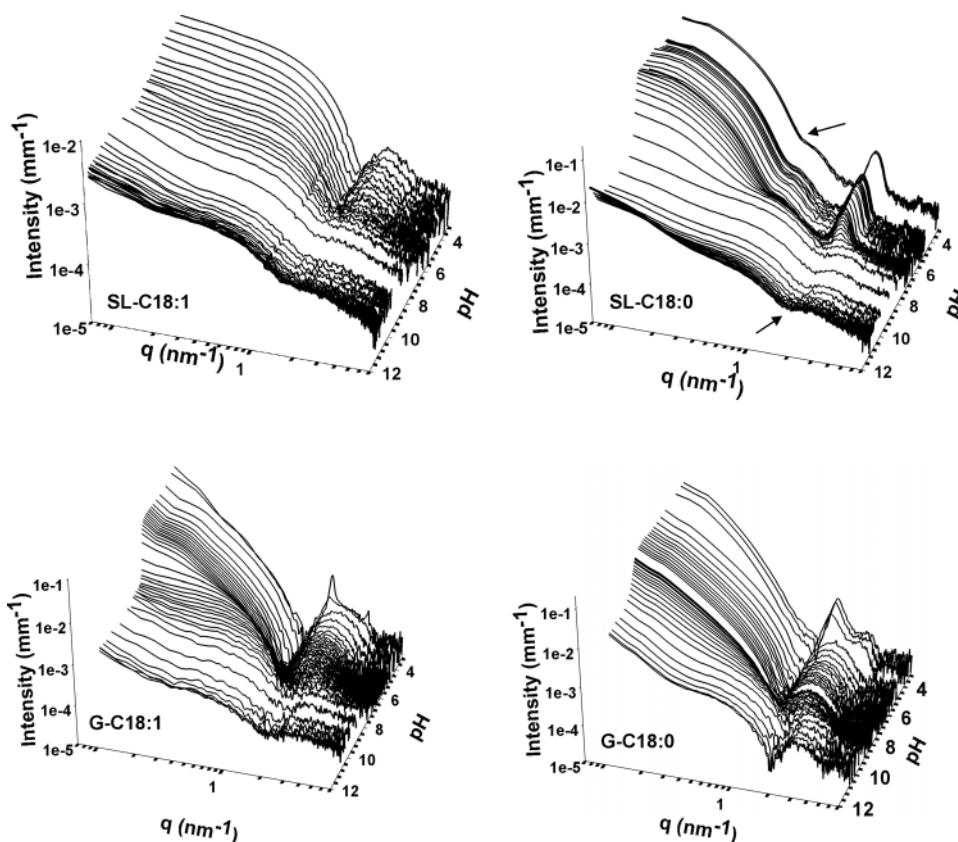
Figure 3. 3D line intensity plots of the pH-resolved SAXS experiments for all glycolipids at 0.5 wt % in water.

the form factor (white arrow) and intense scattering below $q < 1$ nm^{-1}, at pH = ~6.5.

(b) The G-C18:1 system in Figure 3 shows the evolution from the micellar region at pH above 8 to the vesicle domain[39] at acidic pH, characterized by intense scattering at $q < 1$ nm^{-1} and the formation of a broad oscillation at $q > 1$ nm^{-1}. Below pH 4, a white precipitate forms, characterized by a diffraction pattern typical of a lamellar phase.[39] Contour plots of G-C18:1 in Figure S3 visually show the phase transition in the 7.5 < pH < 6 region between the micelles and the vesicles by following the minimum of the form factor (arrow 1) and the appearance of the broad oscillation, attributable to the forming vesicles (arrow 2).

(c) The G-C18:0 system in Figure 3 evolves from a micellar system at basic pH toward a bilayer sheet at acidic pH.[39] As for the G-C18:1, the form factor oscillation at $q > 1$ nm^{-1} (micelle) transforms into a broad oscillation attributable to a bilayer morphology. This is shown in the G-C18:0 contour plot in Figure S3, where one can see that the micelle-to-bilayer transition region is concentrated in a narrow pH range below 8.5.

(d) Finally, the SL-C18:0 system shown in Figure 3 shows a persistent micellar signature until a sharp transition to the twisted ribbon phase occurs, characterized by the appearance of a broad diffraction peak, characteristic of the molecular packing of these molecules within the ribbon plane.[42] The contour plot in Figure S3 shows a direct view of the micelle-to-ribbon transition, the pH of which is situated in the vicinity of pH 7. The ribbon phase is stable down to pH 3, at least.

To better understand which structural parameter drives the morphological changes between the phases at basic and acidic pH, one can plot two model-independent parameters, the fractal dimension, D_f, and the minimum of the form factor oscillation, q_{min}, as well as the model-dependent parameters. The pH-dependent evolution of the micellar fit parameters in the region above $q > 1$ nm^{-1} (Figure 5) can also be used to understand their role in the transitions.

Large-Scale Objects and Evolution of q_{min}. The pH-dependent evolution of the slope at q-values below $q < {\sim}0.7$ nm^{-1} is informative at the morphological transitions on large scales (> ~10 nm). The value of the slope in log−log scale can either be related to a well-defined morphology (e.g., −1 for cylinders, −2 for flat objects)[47] or to fractal objects,[48] even if polydispersity can also influence the value of the slope. Considering our data, we have analyzed the q-region below $q < {\sim}0.3$ nm^{-1} and between ${\sim}0.3 < q$ (nm^{-1}) $< {\sim}0.7$ separately, where these values are to be considered as approximate, the exact ones being indicated in Figure 4. The SL-C18:1 sophorolipid (Figure 4) shows the presence of large scale objects (black line) coexisting with small micelles from basic pH down to pH ~ 7, below which the size of the micelles increases to form cylinders (red line, −1 slope). This result agrees well with published data on this system, where nanoscale platelets coexist with micelles at pH 11,[38] while elongated ellipsoids form below pH 7. The data in Figure 4 show that the platelet aggregates are stable up to the pH ~ 8 point at which elongated micelles are predominant. The concomitant increase in the micellar size (taken here as the radius of gyration) and the change of the oscillation profile of the form factor (refer to the white arrow in SL-C18:1 in Figure S3) suggest that the platelets may act as a reservoir for sophorolipid molecules.
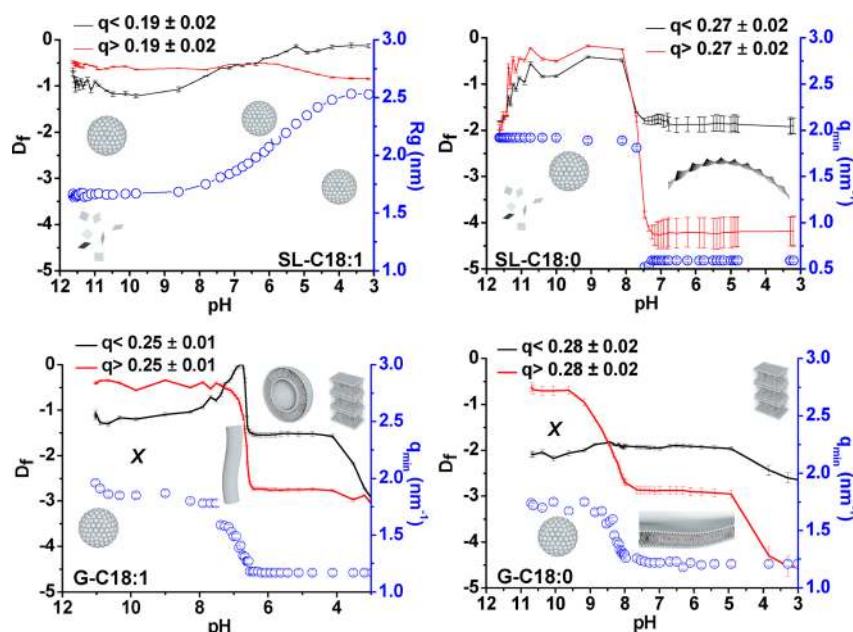
Figure 4. On the left-hand ordinates of each plot is reported the pH-dependent evolution of the fractal dimension, D_f, estimated above and below a critical q-value indicated in each plot and different for each compound. On the right-hand ordinate of SL-C18:1, Rg (radius of gyration) is plotted against pH. For the G-C18:1, G-C18:0, and SL-C18:0 systems, Rg cannot be determined straightforwardly; the minimum of the form factor oscillation, q_{min} (see Figure S2 for more details), as a function of pH is reported, instead, on the right-hand ordinates. "X" refers to the concomitant presence of giant polymorphic structures with micelles in the basic pH region of G-C18:1 and G-C18:0 samples.[39]

The pH-dependent behavior of the monoglucose G-C18:1 drastically changes. At basic pH, the system is formed by micelles and some polymorph giant structures.[39] The slope at low q then gently decreases to zero at pH 7, while a sharp transition takes place below pH 7. Interestingly, q_{min} decreases from about 1.85 to 1.16 nm^{-1} between pH 7 and 8. Remarkably, the q_{min} ratio before and after the transition point is about 1.59, which is close to the theoretical value of 1.43 expected for a transition between full spherical to lamellar objects ($qR = 4.49$ for a sphere and π for a lamellae), if no model assumption is made. Cryo-TEM data show that the micelles fuse together to form giant branched cylindrical micelles in the narrow 7.5 < pH < 6.5 region, as also demonstrated by the D_f value close to −1 in this pH range (Figure 4). After reaching a critical concentration, they then merge into vesicles below pH 6.6,[39] in full consistency with the q_{min} evolution, and the close to −2 value for D_f in the low-q region. This mechanism is further supported by the fact that the transition in q_{min} occurs during the D_f evolution toward −1 and before its stabilization at about −2, thus showing that micelles merge together into cylinders before the morphological evolution from cylinders to vesicles. Finally, the vesicular system is very stable up to pH 4, below which a white lamellar precipitate forms, as indicated by the presence of diffraction peaks in Figure 3.[39]

Upon suppression of the double bond, one forms the G-C18:0 compound, the pH-dependent behavior of which is also shown in Figure 4. At basic pH, this system contains both micelles and giant polymorph structures with a marked −2 slope (black curve), indicating their flat morphology. Interestingly, these objects are very stable and they increase in size and amount upon lowering the pH. This is shown by the constant $D_f = -2$ value below $q < 0.28$ nm^{-1} throughout the pH range, by the slight decrease in q_{min} from about 1.72 to 1.22 nm^{-1} below pH 8, the ratio of which, 1.41, is in very good

agreement with the theoretical 1.43 expected for a sphere-to-lamellae transition. Additional proof for a micelle-to-bilayer transition is given by the increase in D_f above $q > 0.28$ nm^{-1} between pH 9.5 and 8. Differently from G-C18:1, the fact that the increase in D_f occurs at the same time as the q_{min} transition suggests that micelles coalesce and merge together into the infinite, pre-existing, bilayer membrane, without forming intermediate structures. Another hypothesis could also be that micelles act as an external reservoir of matter. The sheets are very stable until pH 4, below which a white lamellar precipitate forms, as indicated by the presence of diffraction peaks in Figure 3 and as discussed elsewhere.[39]

The SL-C18:0 system in Figure 4 shows a hybrid behavior with respect to the other glycolipids. At basic pH, micelles coexist with platelets.[39] Interestingly, the platelets are less stable toward a decrease in pH than in SL-C18:1, as shown by the fast decreasing low-q signal at pH < 10. Upon approaching the transition pH for this system at pH ~ 7.4, the slope undergoes a sharp increase with the simultaneous appearance of the diffraction peak (Figure 3) indicating the formation of twisted ribbons.[42] q_{min} undergoes a large shift from 1.92 to 0.60 nm^{-1} (better highlighted by the arrows in Figure 3) respectively before and after ribbon formation. The latter value corresponds to an indicative size of about 10 nm, a value consistent with the ribbon cross section of about 12−15 nm measured by cryo-TEM.[42] Given the sharp transition between the micelles and the ribbons, one can make the hypothesis that micelles act more as a reservoir of matter for the ribbon than as a real precursor, a hypothesis which will be commented upon later.

pH-Dependent Evolution of Fit Parameters. To go further, we have performed a pH-dependent simulation of the SAXS data using the simple core−shell ellipsoid of revolution model, useful to interpret the structural changes of the micelles with decreasing pH. In Figure 5, we report the shell scattering length density (SLD), ρ_s, the equatorial core radius, R, the
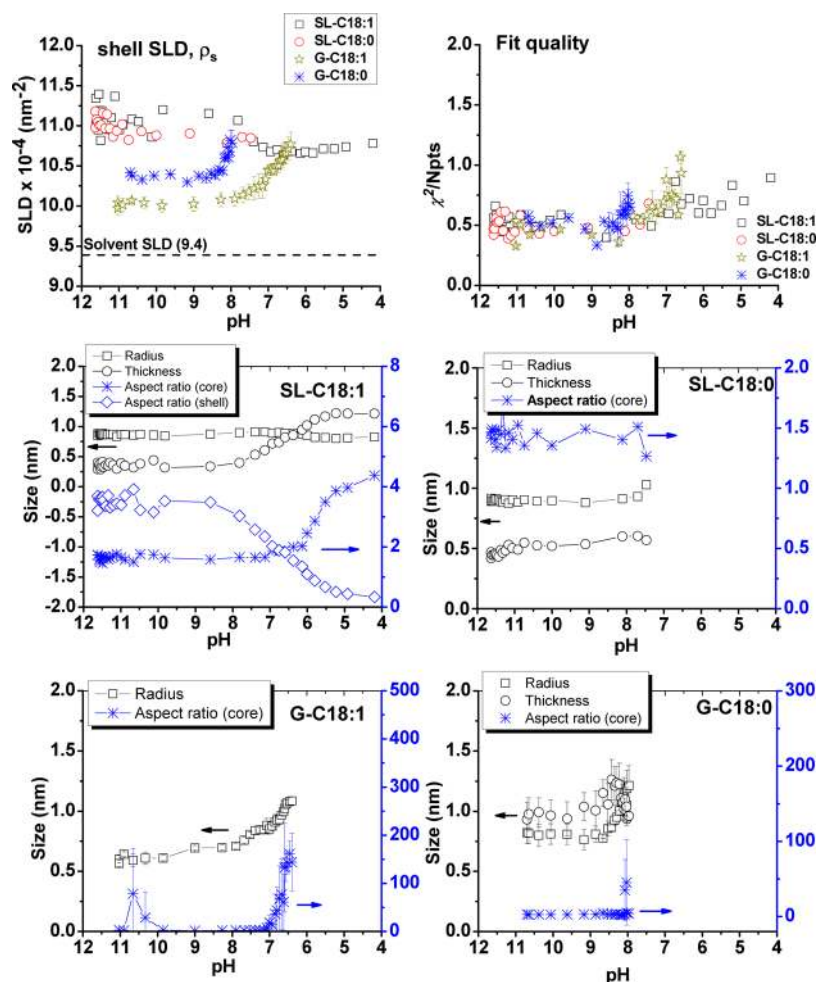
Figure 5. pH-dependent evolution of the core−shell ellipsoid of revolution model fit parameters. SLD, evolution of the fitted shell scattering length density; fit quality, evolution of the $\chi^2/Npts$ quality control parameter. SL-C18:1, SL-C18:0, G-C18:1, G-C18:0 panels: evolution of the core radius, shell thickness (where applicable), and core and shell (where applicable) aspect ratios for the core−shell ellipsoid of revolution form factor model (the details of the model are given in the Supporting Information).

equatorial shell thickness, T, and core and shell aspect ratio along with the $\chi^2/Npts$.

When looking at the data evolution with pH for the SL-C18:1 sophorolipid, one can observe a stable radius and an increasing thickness; interestingly, upon approaching the transition pH 7, the core aspect ratio is strongly enhanced, indicating the formation of elongated micelles, while the shell aspect ratio shrinks to zero. This result is in agreement with previous data collected on salt-containing SL-C18:0 sopho-rolipids in water at pH below 7 under static conditions.[41] The same sample has been used here and in ref 41. This set of data shows a local molecular redistribution within the micelle itself upon decreasing the pH, that is upon increasing the amount of COOH groups; decreasing the amount of COO⁻ groups consequently reduces electrostatic repulsion between the charged carboxylate, and one expects a reduction of the micellar local curvature, the effect of which is a local redistribution of sophorose from the axial to the equatorial region. The intrinsic value of the packing parameter ($p = 0.36$) of SL-C18:1[39] then seems to drive the formation of the elongated micelles at low pH.

The pH-dependent data of glucolipid G-C18:1 shows a 2-fold increase in the radius and an important increase in core aspect ratio, meaning an increase in the ellipsoid length. This

morphological change is in agreement with the formation of giant cylindrical micelles, outlined earlier on the basis of a D_f analysis, and previously shown by means of cryo-TEM data. This continuous evolution of spherical toward cylindrical micelles and eventually vesicles shows the tight structural relationship between the micelles at basic pH and the vesicles at acidic pH.

The saturated glucolipid G-C18:0 shows similar features in terms of radius and thickness evolution, but it also shows that the core aspect ratio is constant throughout the pH range, thus confirming the strong stability of the micelles down to pH 8. This also confirms the previous hypothesis according to which a direct transition from micelles to bilayer membranes occurs without intermediates, probably via a direct micellar fusion or a transfer of amphiphile. Similarly, the pH-independent stability of the micellar structural parameters (Figure 5) for the saturated sophorolipid SL-C18:0 until the formation of the twisted ribbon at pH ∼ 7.4 confirms the hypothesis that in this system micelles play a minor role in the ribbon formation, probably acting as a reservoir of matter. Interestingly, the micelles composed of both saturated compounds, G-C18:0 and SL-C18:0, display the strongest structural stability toward pH changes, if compared to the monounsaturated compounds.
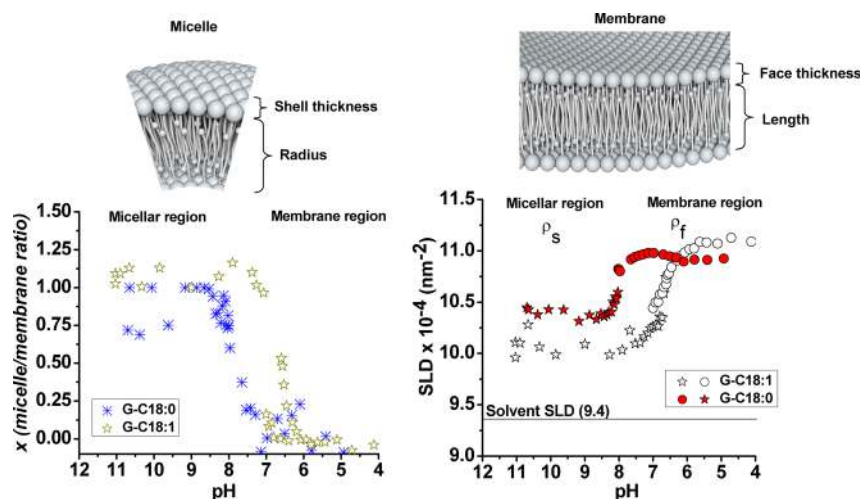
Figure 6. Left-hand panel: pH-dependent evolution of the micelle-to-membrane ratio, x, evaluated using eq S3 and the methodology of which has been given in the Supporting Information. Right-hand panel: pH evolution of the shell SLD, ρ_s, and face SLD, ρ_f, for the G-C18:1 and G-C18:0 glucolipids (0.5 wt %). ρ_s refers to the SLD of a core−shell ellipsoid form factor used to model the data in the micellar stability region and identified by the star symbols. Core radius and shell thickness are additional free variables. ρ_f refers to the SLD of a core−shell bicelle form factor used to model the data in the bilayer membrane stability region and identified by the circle symbols. Face thickness and membrane length have also been set free in the fitting process. More details on the fitting procedure are given in the Supporting Information.

Finally, the most interesting feature for all systems, discussed in detail later, is probably the pH-dependent evolution of ρ_s (Figure 5). In the case of sophorolipids, the starting ρ_s values are comparable for both SL-C18:1 and SL-C18:0 samples and higher than those for the glucolipids. In addition, ρ_s for sophorolipids seems to decrease with decreasing pH, while it clearly increases for glucolipids in the vicinity of the corresponding transition pH values.

The drawback of the data in Figure 5 is the limited validity of the ellipsoid model in the vicinity of the transition pH for all systems except SL-C18:1. To confirm the ρ_s trends, we have also modeled the bilayer region below the transition pH. Figure 6 shows the pH-driven evolution of the micelle/membrane ratio (x, in eq S3) between unity (micelles only) and zero (membrane only) with decreasing pH, nicely demonstrating the quantitative morphological evolution from micelles to bilayer membranes (vesicles or sheets). As for the corresponding SLD, the pH-dependent evolution of ρ_s (the shell SLD in the ellipsoids) and ρ_f (the face SLD in the bilayer) combined in a single set of data before and after the transition pH value is also plotted in Figure 6. These data confirm and actually complete the evolution presented in Figure 5: the pH-dependent increase of the SLD in the hydrophilic region for the glucolipid compounds.

SLD of the hydrophilic region (shell or face) is strongly sensitive to hydration in both the ellipsoid and bicelle models: upon hydration, the value of SLD decreases, while upon dehydration, SLD increases. According to the data presented in Figure 5 and Figure 6, it seems that the hydrophilic shell/water palisade undergoes dehydration in both glucolipids when pH decreases, while the opposite occurs in the presence of sophorose. We believe that, under basic pH conditions, the presence of the carboxylate group, besides influencing the local curvature due to electrostatic repulsion, also contributes to the hydrophilicity of the carbohydrate shell in all compounds, also due to the presence of the sodium counterion, which brings between 4 and 8 water molecules;[49] monosaccharides like glucose are known to have a small hydration number, less than 3,[50,51] while this value was estimated to be above 18 for

sophorolipids in acidic pH medium in the presence of RbCl.[41] These assumptions indicate that, upon lowering the pH and subsequent formation of COOH groups, the contribution of sodium to carbohydrate hydration becomes less important, and under these conditions, one can reasonably expect the natural hydration layer of the sugar to become the main source of structural water, which is higher for sophorose than glucose, as it results from the SLD trends. In pH-responsive lipidic systems, similar arguments have been specifically used to explain lamellar (low curvature) to hexagonal (high curvature) phases. Li et al.[52] have developed a model for anionic lipids mixed either with neutral or cationic lipids showing that the pH-dependent instability of vesicles is highly dependent on the membrane composition and in particular on the flow of counterions and their hydration shell. When these move away from the surface, the bilayer curvature decreases because the effective surface area of the lipid decreases. When hydrated counterions approach the surface, on the contrary, higher curvatures are stabilized. Their model fits well both previous experimental results by Hafez et al.[53,54] and our own data, which can be considered to come from a mixture of an anionic (COO−Na+) and neutral (COOH) lipid mixture, of which the composition continuously evolves with pH. The mechanical deformation of lipid membranes due to water addition/removal has been known for a long time under the name of "osmotic stress", first described by LeNeveu[55] in 1977 for lecithin bilayer and later exploited by many other authors.[14,56,57] In particular, Rand et al.[14] have shown that a variation of osmotic pressure is also able to modify the curvature radius of a lipid bilayer from lamellar to hexagonal, thus explaining from a fundamental point of view Li's[52] model and, most likely, our own data.

In view of the discussion above, we then believe that the stronger water-withdrawing effect induced by pH in the glucose-based compounds contributes, at the same time as the reducing inter-COO− electrostatic repulsion and Na+ removal, to decrease the effective area per headgroup. Under these conditions, the hydrophilic headgroups come closer together. According to the simple packing parameter model, one can explain the formation of objects with a lower curvature,

as this is the case for the lipid membranes with respect to the starting micelles. The calculated packing parameter for G-C18:1 is about 0.72,[39] which, combined with an additional water-withdrawing effect occurring during lowering the pH, can largely explain the micelle-to-cylinder-to-vesicle transition observed for this compound. However, the sudden bilayer formation and the strong stability of the micellar regime observed for G-C18:0 cannot be explained using these arguments. The different behavior in the structural evolution in the vicinity of the transition pH between these two systems is also clear from the plot of the micelle and membrane structural parameters (radius vs shell thickness and length vs face thickness), the details of which are given in the Supporting Information. Figure S4 shows a nice, continuous overlap between the micellar radius ($\sim$0.6 nm) and shell thickness ($\sim$0.8 nm) with the bilayer membrane length ($\sim$1 nm) and respective face thickness ($\sim$1 nm) with pH for the G-C18:1 sample. On the contrary, a clear structural evolution inconsistency exists between the micellar radius and shell thickness with respect to the bilayer membrane length and face thickness for the G-C18:0 sample. Both samples can be described by an interdigitated bilayer, because the its size (about 3 nm) is comparable with the typical molecular dimensions, as discussed in the Supporting Information.

Formation of Bilayer Structures. G-C18:1 and G-C18:0 samples share a similar local bilayer structure, although the former assembles into a vesicle while the latter into an infinite bilayer. The assemblying pathway is also different. Micelles composed of G-C18:1 fuse into wormlike objects which in turn merge into disks; on the contrary, micelles composed of G-C18:0 are stable toward pH and serve as a reservoir for the infinite growth of a pre-existing flat structure. If a common point is the presence of a flat bilayer at a given pH, characteristic for each molecule, what is the driving force that induces the disk bending in the G-C18:1 case and disk growth for G-C18:0? We should recall that this behavior is valid at room temperature, that is, above and below the oleic acid and stearic acid melting temperatures, respectively (13 °C for oleic and 69 °C for stearic acid), the fatty acid components of, respectively, G-C18:1 and G-C18:0.[39]

To attempt to explain the pH-dependent behavior of these two compounds at room temperature, one could refer to the work by Leng et al.,[17] who elegantly explained the micelle-to-vesicle transition mechanism in a lecithin−bile salt binary system. They have shown how this is overall governed by kinetics but, at a local scale, by the lecithin (neutral)/bile salt (charged) ratio and salt concentration. They discuss the role of bile salt as an "edge-actant", an edge stabilizing agent,[58] responsible for the stability of the bilayer membrane toward growth and, eventually, closure into vesicles. Bile salt preferentially sits at and stabilizes the outer edges of the lecithin membrane, contributing to reduce the local line tension, caused by the exposure of the hydrophobic chain of lecithin to the aqueous environment. The interplay between the lecithin-rich membrane disk growth and increase in line tension governs the instability of the disk at its edge and consequently the closure into a vesicle. Authors define a vesiculation index, V_f, which is proportional to the membrane radius and line energy and inversely proportional to the bending energy of the membrane. For $V_f < 1$, flat membranes are stable, but for $V_f > 2$, vesicles become stable. In between, both membranes and vesicles are stable. Qualitatively, vesicles form whenever the bending energy of the membrane is small, that is, for elastic,

flexible, objects, and upon growth (large membranes are easier to bend). To this logic phenomenon, one should add the contribution of line tension; at high values of line tension, V_f increases and vesicles form, occurring for those systems in which no edge rim stabilizes the membrane: vesicle formation is then preferred toward a stable membrane. If, for a given compound, the bending energy is constant while the membrane radius evolves with time, the edge stability will depend on the area fraction of edge-actant in the rim (which will in turn depend on the volume fraction of the edge-actant in solution) and salt concentration. Large amounts of edge-actants in the rim stabilize the rim itself by exposing the charged hydrophilic headgroups toward the solvent, instead of the lecithin hydrocarbon chains, while large amounts of salt screen the electrostatic repulsions between the edge-actant (charged) headgroups, thus contributing even more to membrane edge stability. Leng et al. could show that for large amounts of area fraction occupied by bile salt (the edge-actant) in a lecithin-composed membrane, and for a given salt concentration, the membrane becomes highly stable even at radii as large as 200 nm (very small V_f values). The higher the salt in solution, the more stable the membrane.

If we apply the main conclusions of the above study to the glucolipid systems presented here, provided certain hypotheses developed in the Supporting Information, we find one strong analogy: the pH variation practically imposes a continuous evolution in the COOH (neutral)/COO$^-$Na$^+$ (charged) proportion in solution, a parameter which is analogous to the lecithin (neutral)/bile salt (charged) ratio described by Leng et al.[17] At pH > 10 (100% ionization degree of the fatty acid), both G-C18:1 and G-C18:0 systems are composed by more than $\sim$95% (by number) of micelles, as estimated by the micelle/membrane ratio customized model (eq S3) used to generate the data in Figure 6. The remaining $\sim$5% account for large objects responsible for the low-q scattering signal present in Figure 2. Data in Figure 2 and Table S1 also show that G-C18:0 is able to stabilize highly curved, spherical, micellar aggregates, while the presence of a saturated double bond (G-C18:1) destabilizes the system enough to form slightly ellipsoidal objects. By increasing the COOH/COO$^-$Na$^+$ ratio, the difference between both systems becomes more pronounced as G-C18:1 continuously forms infinitely long cylindrical micelles (strong increase in aspect ratio (core) in Figure 5 and D_f approaching −1 in Figure 4), while micelles are stable and remain spherical in the G-C18:0 system (constant core aspect ratio in Figure 5). These differences indicate that the high flexibility of the hydrophobic core for G-C18:1 (room temperature, RT > T_M of oleic acid, 13 °C), the smaller inter-COO$^-$ repulsion contribution, and the decreasing surface area per hydrophilic headgroup due to water-withdrawing effects permit the unidimensional micellar growth. On the contrary, the stiffer saturated fatty acid (RT $\ll T_M$ of stearic acid) does not allow the same core flexibility and spherical micelles are eventually more resistant toward the COOH/COO$^-$Na$^+$ ratio and hydration evolution. However, at a critical COOH/COO$^-$Na$^+$ composition, a sharp morphological transition must take place to reduce the system energy and to take into account the new geometrical constraints. Below the respective transition pH, each glucolipid finds itself in a membrane geometry; however, G-C18:1 forms vesicles ($V_f > 2$), while G-C18:1 infinitely grows into large sheets ($V_f < 1$). If one relies on the model in ref 17, two parameters play a crucial role in this system, the bending energy and line tension. The use of a
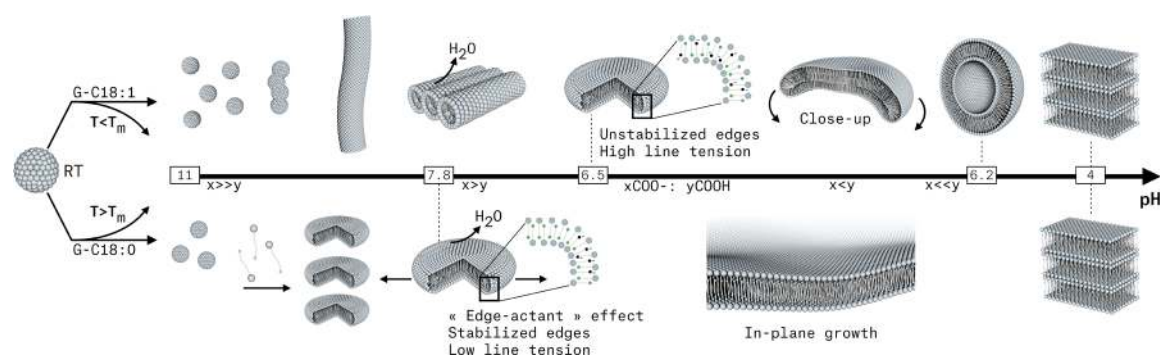
Figure 7. Scheme illustrating the pH-driven self-assembly of G-C18:1 and G-C18:0 glucolipids in water at room temperature. x and y represent the fraction of COO⁻ and COOH groups during pH change. Unless otherwise indicated, experiments have been done at room temperature (RT). The T_m for oleic acid (contained in G-C18:1) is 13 °C, while the T_m for stearic acid (contained in G-C18:0) is 69 °C.
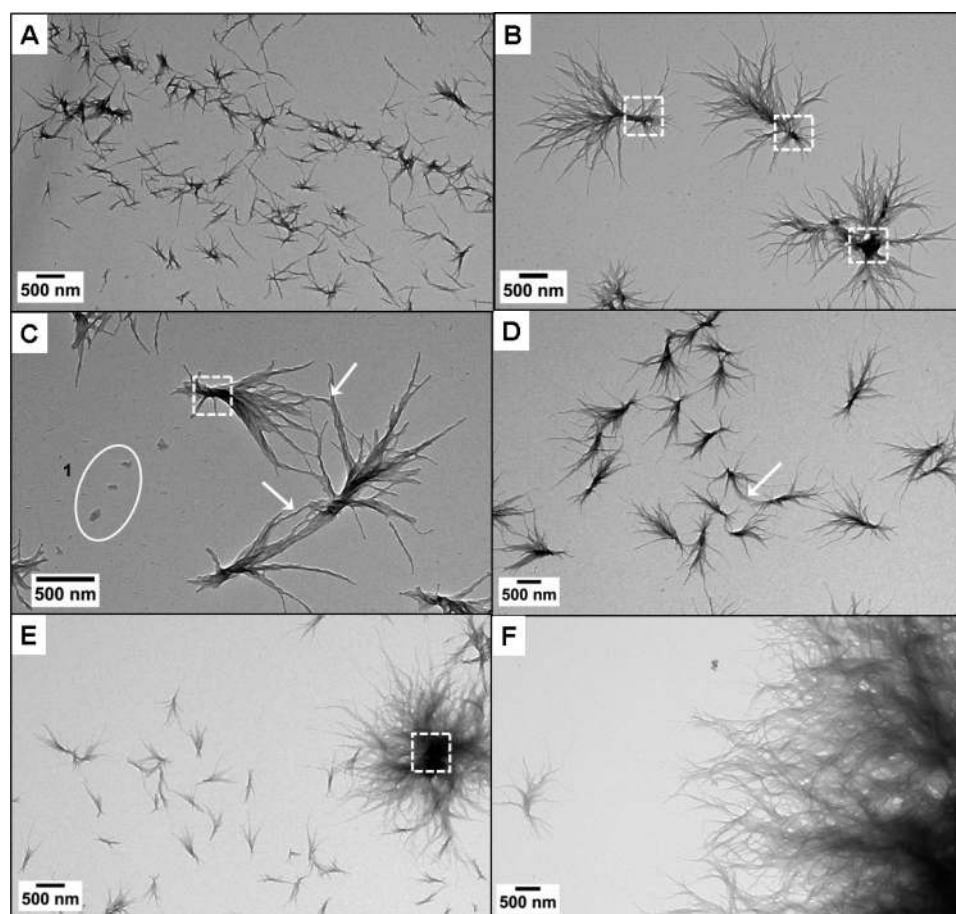

Figure 8. TEM images collected on a copper TEM grid containing a drop of SL-C18:1 sample at pH 11 (0.5 wt %) and locally exposed for a few seconds to a 0.1 M HCl solution. The drop is immediately dried, and the grid is analyzed as such. All images come from the same grid, and they have been tried to be collected in the grid region at the opposite of the point of injection of HCl.

saturated fatty acid (stearic acid in G-C18:0) with a high melting temperature (69 °C) compared to room temperature seems to be responsible for the formation of a highly stable bilayer membrane, stiff and with a high bending energy, contributing to reduce V_f. Meanwhile, the line tension must also be very small to account for such stable sheet structures even for "infinite" membrane radii. This is possible for an important concentration of charged species at the edges of the membrane covering an important rim area fraction. The G-C18:0 system seems to better accommodate to high curvatures (at the rim) than G-C18:1, as also demonstrated by the fact

that G-C18:0 forms highly stable spherical micelles, while G-C18:1 forms ellipsoidal and cylindrical objects; we then make the hypothesis that the membrane edges in the G-C18:0 system are rich in COO⁻Na⁺, thus preventing high line tension and consequent closing of the sheet into a vesicle. On the contrary, the amount of COO⁻Na⁺ in the G-C18:1 system is most likely diluted throughout the membrane rather than being localized at the rim, the main reason being the higher fluidity of the oleic acid tail, the T_M of which is lower than room temperature. These mechanisms are summarized in Figure 7.
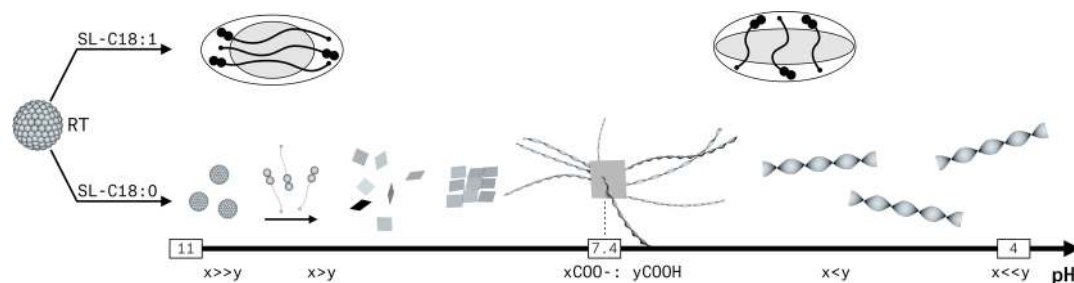
Figure 9. Scheme illustrating the pH-driven self-assembly of SL-C18:1 and SL-C18:0 glycolipids in water at room temperature. x and y represent the fraction of COO$^-$ and COOH groups during pH change.

This hypothesis does not explain all of our observations. At pH values below 5–6, the overall content of COO$^-$Na$^+$ glucolipid species becomes very small and vesicles should form for all systems, which is not the case. To explain this phenomenon, we speculate that a critical radius exists and above which the bilayers are so large that even for high line tension, the energetic cost to bend them into a vesicle is so high that the flat membrane configuration is still preferred. We should emphasize the fact that, below pH 5, the G-C18:0 sheets precipitate into a lamellar phase, just as found for G-C18:1. This effect seems to go in the sense of the previous hypothesis. In the G-C18:1 system, the residual COO$^-$Na$^+$ are homogeneously distributed in the entire bilayer membrane, helping to stabilize the vesicle mild curvature, as observed in ref 17 for diluted bile salt systems. When all carboxylate groups are protonated, the vesicle curvature becomes so small that a lamellar phase eventually precipitates. Finally, we must recall that, if these experiments are performed at $T < 13$ °C, G-C18:1 forms flat bilayer sheets, while, if performed at $T > 69$ °C, G-C18:0 forms vesicles,[39] thus showing the direct importance of membrane flexibility in relationship with the fluidity of the hydrophobic region. Even though this is not a direct proof, these additional data suggest that, if the mobility of the charged lipids within the membrane is affected, it is possible to control their local concentration and eventually the long-range curvature of the bilayer membrane. This was shown by other authors. Madenci et al.[59] have built a model on lecithin and bile salt mixtures confirming Leng's observations and, at least from a qualitative point of view, they do show that the end-caps of bilayer disks are richer in bile salt, while lecithin is distributed in the bilayer. Other works on catanionic surfactant mixtures also imply partitioning of lipids at a molecular level, as proposed in refs 60–62 and shown by means of contrast matching small angle neutron scattering.[61]

Additional Insights into the Mechanisms of Formation. Superimposing the pH-dependent SAXS data presented in Figure 3 shows an interesting, very unique feature: practically all systems have at least one value of the wavevector q which is constant throughout the variation in pH. This invariant is commonly called the "isoscattering", or "isosbestic scattering", point. Even if a similar scattering behavior has been reported for several systems both in SAXS[63,64] and XRD[65] studies, for instance, in heat-induced aggregation and gelation of β-lactoglobulin and ovalbumin mixtures,[63] or temperature-induced structural modification of poly(N-isopropylacrylamide) hydrogels, the real significance of an isoscattering point, although generally attributed to microphase separation processes, is still unclear, and in particular the meaning of the isoscattering q-value itself (please refer to the Supporting Information for more details). In spite of a better interpretation

of isoscattering points in the literature, we apply the formation of stable "nanopockets" (synonym term to microdomain employed in ref 64) reported in the literature to the systems studied here. The SL-C18:0 system displays a narrow q_{iso} interval (Figure S5) centered at 0.56 nm^{-1} (11.21 nm), corresponding to the size of several micellar aggregates (at basic pH) and, approximately, the cross section of a single ribbon.[42,38] We speculate that the presence of an isoscattering point could also indicate the existence of a nucleation and growth mechanism starting from the nanopockets formed at basic pH. This hypothesis seems to be confirmed by complementary standard TEM analysis performed on a grid on which the initial ribbon growth stages has been quenched (see the Materials and Methods for details). Figure 8A–D presents a large number of fibrillar objects of which the size does not exceed a few micrometers. Meanwhile, in Figure 8E,F, larger objects compose a dense network of entangled fibers. The entire set of images nicely demonstrates the fact that the same grid contains SL-C18:0 fibers at an early (A–D) and late (E,F) stage of formation. A closer look at Figure 8A–D illustrates the presence of a large number of aggregates all having a point in common: each one has a "bouquet"-like morphology, with a dense elongated center (dotted squares in Figure 8B,C) and a fibrillar ramification on both extremities. The arrows in Figure 8C,D draw the attention on how these "bouquet"-like aggregates connect together via their fibrillar ramifications to eventually form a broader network (Figure 8D). Objects with a high fibrillation density in Figure 8E show that their development can also occur on a single nucleation site, which can phagocytize nearby germs. Eventually, midsized fibrillar pellets indefinitely grow by both fibrillation and aggregation into very large aggregates (Figure 8E). The presence of large spherical fibrous pellets has been demonstrated before in cryo-TEM experiments collected on as-synthesized SL-C18:0 sample at acidic pH,[43] thus indicating that the observation method preferred in this work does not influence the formation mechanism of the fibers.

At basic pH, the SL-C18:0 is composed of micelles and, in minor amounts, of platelets. Two hypotheses can then be formulated. Clusters of micelles start to form upon lowering the pH, becoming the nucleation point of the fibers. The core size of the nucleation point/nanopocket would remain constant, thus providing the isoscattering point in SAXS experiments. This mechanism seems to be in line with previously reported mechanisms for amyloid fibrillogenesis and in which micellar aggregates are believed to be both the nucleation point and reservoir.[66–68] However, one can wonder which is the driving force for micelles to spontaneously aggregate into nanopockets. To overcome this question, we formulate a second hypothesis according to which the platelets constitute the seed from which

the fibers nucleate and develop. Against this hypothesis, one should highlight the fact that the platelet aggregates disappear with lowering pH, as shown by the diminishing low-q signal between pH 12 and pH 10 on the SL-C18:0 sample in Figure 4. However, that signal is related to large (several micrometers) platelet aggregates and not to a single platelet, as shown in ref 38. On the contrary, other arguments support the second hypothesis. Similarities are found in the formation of twisted/helical ribbons from gemini surfactant systems, which form platelets in the presence of a racemate mixture of D-, L-tartrate counterions but form ribbons in the enantiomeric excess of one or the other.[13] More generally, recent studies on the fibrillation mechanism of silk fibers (using SAXS/WAXS/Raman),[69] peptide nanotubes (using SAXS, cryo electron tomograghy, and cryo TEM),[16] and amyloid fibers (Monte Carlo simulation)[70] all seem to exclude the nucleation process from micelles but rather converge toward an aggregation/conversion (for silk and amyloid) or oriented attachment (peptide nanotubes) set of mechanisms. We conclude then that micelles, present at basic pH, serve as a reservoir of matter but not as nucleation points. This is shown in the scheme in Figure 9, which also reports the micellar structural evolution for the SL-C18:1 sophorolipids for a matter of comparison.

■ CONCLUSION

This work unravels the pH-dependent self-assembly mechanism of a set of four glycolipids bearing a single glucose and a sophorose headgroup and oleic, or stearic, acid as lipid backbone. These structurally related compounds are obtained directly, or indirectly, from the fermentation process of the yeast *Starmerella bombicola*. All four compounds form spherical, or ellipsoidal, micelles under basic pH conditions due to the strong electrostatic repulsion between the COO⁻ groups. The structures of the micelles mainly vary in terms of the glycolipid distribution within the micelle itself. Upon lowering the pH of the solution, each glycolipid follows its own pathway toward different structures. We have used pH-resolved *in situ* SAXS using synchrotron radiation to follow the morphological changes; the SAXS data have been thoroughly analyzed using both a model-independent and a model-dependent approach. The pH-dependent analysis of the slope in the low-q region informs on the nature of the large aggregates, while the evolution of the minimum of the form factor oscillation, q_{min}, informs on the morphology changes. Then, we have modeled the micellar region using a core–shell ellipsoid of revolution form factor using an inhomogeneous shell, necessary to fit part of the data. Finally, when appropriate, we have used a core–shell bicelle model to fit the membrane morphologies (vesicle, bilayer).

We find the following:

- G-C18:1 system: Micelles are ellipsoids at basic pH, and they elongate and merge into cylindrical and wormlike objects, which in turn fuse into large disks in the narrow pH region between 7.5 and 6.5., where glucolipids are interdigitated. This is promoted by (1) the fluid hydrophobic region (RT > T_m), (2) the intrinsic value of the packing parameter (0.72), and (3) the dehydration process. (4) High line tension at the disk extremities promoting vesicle formation at pH < 6.2. (5) Formation of a lamellar phase below pH 4, presumably when all COO⁻ turn into COOH.

- G-C18:0 system: Micelles are spherical and very stable in a broad pH region. They coexist with a small fraction (about 5%) of large flat objects which experience a sudden increase in size below the transition pH 8, where glucolipids are interdigitated. Micelles either fuse in the preformed membranes or dissolve to provide matter for the bilayer growth. In all cases, they seem to act as a reservoir. The bilayer does not bend into vesicles, but it rather grows infinitely into extended bilayers, possibly because of the edge-stabilizing effect of the edge-actants, composed of the residual glucolipid bearing a COO⁻ group. A lamellar phase eventually precipitates presumably when all COO⁻ groups are replaced by COOH.

- SL-C18:1 system: Micelles are ellipsoids with a given sophorolipid distribution inside. Upon lowering the pH, the chain fluidity, the strong hydration of sophorose, and the packing parameter (0.36) drive the formation of elongated ellipsoids, although with a different distribution of sophorolipids inside, thus forming coffee-bean-like objects.[41] If platelets are also reported to coexist with micelles at basic pH,[43] they disassemble with lowering the pH and serve as a source of matter for micelle rearrangement.

- SL-C18:0 system: Micelles are spherical stable objects until the transition pH. The formation of the ribbons occurs at pH 7.4 from, we believe, preformed nanoscale platelets serving as nucleation points.[43] Micelles serve as a source of matter for ribbon formation. The driving force for ribbon formation is still unclear, but it could be related to the bulky sophorose perturbation effect during the formation of a flat bilayer.

In the end, this work is a didactical illustration of the complexity of the self-assembly process of a stimuli-responsive amphiphile and during which many concomitant parameters play a key role at different stages of the process. We believe that this work should provide a step forward in the prediction of such complex systems.

■ ASSOCIATED CONTENT

ⓢ Supporting Information

The Supporting Information is available free of charge on the ACS Publications website at DOI: 10.1021/acs.langmuir.6b02337.

(Figure S1) HPLC-ELSD chromatogram of the SL-C18:1 compound and description of the strategy to fit the SAXS data; (Figure S2) the general overview of the treatment performed on a typical SAXS spectrum; (Figure S3) the contour plots of the pH-resolved SAXS experiments for all glycolipids; (Figure S4) the pH-dependent evolution of the micelle and membrane bilayer structural parameters for G-C18:1 and G-C18:0 samples obtained after fitting the SAXS data; (Figure S5) the isoscattering point for SL-C18:0; (Table S1) the parameters used to fit the SAXS data presented in Figure 2; also the hypotheses for applying Leng's model to the G-C18:1 and G-C18:0 systems (PDF)

■ AUTHOR INFORMATION

Corresponding Author
*E-mail: niki.baccile@upmc.fr.

Notes

The authors declare no competing financial interest.

■ ACKNOWLEDGMENTS

■ REFERENCES

(1) Felber, E.; Dufresne, M.-H.; Leroux, J.-C. pH-sensitive vesicles, polymeric micelles, and nanospheres prepared with polycarboxylates. *Adv. Drug Delivery Rev.* **2012**, *64*, 979−992.

(2) Brown, P.; Butts, C. P.; Eastoe, J. Stimuli-responsive surfactants. *Soft Matter* **2013**, *9*, 2365−2374.

(3) Li, X.; Yang, Y.; Eastoe, J.; Dong, J. Rich Self-Assembly Behavior from a Simple Amphiphile. *ChemPhysChem* **2010**, *11*, 3074−3077.

(4) Du, J.; Tang, Y.; Lewis, A. L.; Armes, S. P. pH-Sensitive Vesicles Based on a Biocompatible Zwitterionic Diblock Copolymer. *J. Am. Chem. Soc.* **2005**, *127*, 17982−17983.

(5) Morigaki, K.; Walde, P. Fatty acid vesicles. *Curr. Opin. Colloid Interface Sci.* **2007**, *12*, 75−80.

(6) Israelachvili, J. N.; Mitchell, D. J.; Ninham, B. W. Theory of self-assembly of hydrocarbon amphiphiles into micelles and bilayers. *J. Chem. Soc., Faraday Trans. 2* **1976**, *72*, 1525−1568.

(7) Nagarajan, R.; Ruckenstein, E. Theory of Surfactant Self-Assembly: A Predictive Molecular Thermodynamic Approach. *Langmuir* **1991**, *7*, 2934−2969.

(8) Berr, S. S.; Caponetti, E.; Johnson, J. S., Jr.; Jones, R. R. M.; Magid, L. J. Small-angle neutron scattering from hexadecyltrimethylammonium bromide micelles in aqueous solutions. *J. Phys. Chem.* **1986**, *90*, 5766−5770.

(9) Alexandridis, P.; Athanassiou, V.; Fukuda, S.; Hatton, T. A. Surface Activity of Poly(ethy1eneoxide)-block-Poly(propy1ene oxide)-block-Poly(ethy1eneoxide) Copolymers. *Langmuir* **1994**, *10*, 2604−2612.

(10) Klijn, J. E.; Stuart, M. C. A.; Scarzello, M.; Wagenaar, A.; Engberts, J. B. F. N. pH-Dependent Phase Behavior of Carbohydrate-Based Gemini Surfactants. The Effects of Carbohydrate Stereochemistry, Head Group Hydrophilicity, and Nature of the Spacer. *J. Phys. Chem. B* **2007**, *111*, 5204−5211.

(11) Nagarajan, R. Molecular Packing Parameter and Surfactant Self-Assembly: The Neglected Role of the Surfactant Tail. *Langmuir* **2002**, *18*, 31−38.

(12) Zana, R. Gemini (dimeric) surfactants. *Curr. Opin. Colloid Interface Sci.* **1996**, *1*, 566−571.

(13) Oda, R.; Huc, I.; Schmutz, M.; Candau, S. J.; MacKintosh, F. C. Tuning bilayer twist using chiral counterions. *Nature* **1999**, *399*, 566−569.

(14) Rand, R. P.; Fuller, N. L.; Gruner, S. M.; Parsegian, V. A. Membrane Curvature, Lipid Segregation, and Structural Transitions for Phospholipids under Dual-Solvent Stress? *Biochemistry* **1990**, *29*, 76−87.

(15) Guida, V. Thermodynamics and kinetics of vesicles formation processes. *Adv. Colloid Interface Sci.* **2010**, *161*, 77−88.

(16) Cenker, C. C.; Bomans, P. H. H.; Friedrich, H.; Dedeoglu, B.; Aviyente, V.; Olsson, U.; Sommerdijk, N. A. J. M.; Bucak, S. Peptide nanotube formation: a crystal growth process. *Soft Matter* **2012**, *8*, 7463.

(17) Leng, J.; Egelhaaf, S. U.; Cates, M. E. Kinetics of the Micelle-to-Vesicle Transition: Aqueous Lecithin-Bile Salt Mixtures. *Biophys. J.* **2003**, *85*, 1624−1646.

(18) Genc, R.; Ortiz, M.; O'Sullivan, C. K. Curvature-Tuned Preparation of Nanoliposomes. *Langmuir* **2009**, *25*, 12604−12613.

(19) Bryskhe, K.; Bulut, S.; Olsson, U. Vesicle Formation from Temperature Jumps in a Nonionic Surfactant System. *J. Phys. Chem. B* **2005**, *109*, 9265−9274.

(20) Corti, M.; Cantù, L.; Brocca, P.; Del Favero, E. Self-assembly in glycolipids. *Curr. Opin. Colloid Interface Sci.* **2007**, *12*, 148−154.

(21) John, G.; Masuda, M.; Okada, Y.; Yase, K.; Shimizu, T. Nanotube formation from Renewable Resources via Coiled Nanotubes. *Adv. Mater.* **2001**, *13*, 715−718.

(22) Garamus, V. M.; Milkereit, G.; Gerber, S.; Vill, V. Micellar structure of a sugar based bolaamphiphile in pure solution and destabilizing effects in mixtures of glycolipids. *Chem. Phys. Lett.* **2004**, *392*, 105−109.

(23) Desai, J. D.; Banat, I. M. Microbial production of surfactants and their commercial potential. *Microbiol. Mol. Biol. Rev.* **1997**, *61*, 47−64.

(24) Shimizu, T. Molecular Self-Assembly into One-Dimensional Nanotube Architectures and Exploitation of Their Functions. *Bull. Chem. Soc. Jpn.* **2008**, *81*, 1554−1566.

(25) Jung, J. H.; Shinkai, S.; Shimizu, T. Spectral Characterization of Self-Assemblies of Aldopyranoside Amphiphilic Gelators: What is the Essential Structural Difference between Simple Amphiphiles and Bolaamphiphiles. *Chem. - Eur. J.* **2002**, *8*, 2684−2690.

(26) Kitamoto, D.; Morita, T.; Fukuoka, T.; Konishi, M.; Imura, T. Self-assembling properties of glycolipid biosurfactants and their potential applications. *Curr. Opin. Colloid Interface Sci.* **2009**, *14*, 315−328.

(27) Fuhrhop, J.-H.; Wang, T. Bolaamphiphiles. *Chem. Rev.* **2004**, *104*, 2901−2937.

(28) Kamiya, S.; Minamikawa, H.; Jung, J. H.; Yang, B.; Masuda, M.; Shimizu, T. Molecular Structure of Glucopyranosylamide Lipid and Nanotube Morphology. *Langmuir* **2005**, *21*, 743−750.

(29) Axford, J. The impact of glycobiology on medicine. *Trends Immunol.* **2001**, *22*, 237.

(30) Dwek, R. A. Glycobiology: Toward Understanding the Function of Sugars. *Chem. Rev.* **1996**, *96*, 683−720.

(31) Kameta, N.; Minamikawa, H.; Masuda, M. Supramolecular organic nanotubes: how to utilize the inner nanospace and the outer space. *Soft Matter* **2011**, *7*, 4539.

(32) Marchant, R.; Banat, I. Biosurfactants: a sustainable replacement for chemical surfactants? *Biotechnol. Lett.* **2012**, *34*, 1597−1605.

(33) Marchant, R.; Banat, I. Microbial biosurfactants: challenges and opportunities for future exploitation. *Trends Biotechnol.* **2012**, *30*, 558−565.

(34) Van Bogaert, I. N. A.; Saerens, K.; De Muynck, C.; Develter, D.; Soetaert, W.; Vandamme, E. J. Microbial production and application of sophorolipids. *Appl. Microbiol. Biotechnol.* **2007**, *76*, 23−34.

(35) Roelants, S. L.; Ciesielska, K.; De Maeseneire, S. L.; Moens, H.; Everaert, B.; Verweire, S.; Denon, Q.; Vanlerberghe, B.; Van Bogaert, I. N. A.; Van der Meeren, P.; Devreese, B.; Soetaert, W. Towards the industrialization of new biosurfactants: Biotechnological opportunities for the lactone esterase gene from *Starmerella bombicola*. *Biotechnol. Bioeng.* **2016**, *113*, 550−559.

(36) Masuda, M.; Yozac, K.; Shimizu, T. Polymorphism of monolayer lipid membrane structures made from unsymmetrical bolaamphiphiles. *Carbohydr. Res.* **2005**, *340*, 2502−2509.

(37) Frankel, D. A.; O'Brien, D. F. Supramolecular Assemblies of Diacetylenic Aldonamides. *J. Am. Chem. Soc.* **1994**, *116*, 10057−10069.

(38) Cuvier, A.-S.; Babonneau, F.; Berton, J.; Stevens, C. V.; Fadda, G. C.; Péhau-Arnaudet, G.; Le Griel, P.; Prévost, S.; Perez, J.; Baccile, N. Nanoscale platelet formation by monounsaturated and saturated sophorolipids under basic pH conditions. *Chem. - Eur. J.* **2015**, *21*, 19265−19277.

(39) Baccile, N.; Selmane, M.; Le Griel, P.; Prévost, S.; Perez, J.; Stevens, C. V.; Delbeke, E.; Zibek, S.; Guenther, M.; Soetaert, W.; Van Bogaert, I. N. A.; Roelants, S. pH-driven self-assembly of acidic microbial glycolipids. *Langmuir* **2016**, *32*, 6343.

(40) Baccile, N.; Babonneau, F.; Jestin, J.; Pehau-Arnaudet, G.; Van Bogaert, I. Unusual, pH-induced, self-assembly of sophorolipid biosurfactants. *ACS Nano* **2012**, *6*, 4763−4776.

(41) Manet, S.; Cuvier, A.-S.; Valotteau, C.; Fadda, G. C.; Perez, J.; Karakas, E.; Abel, S.; Baccile, N. Structure of Bolaamphiphile Sophorolipid Micelles Characterized with SAXS, SANS, and MD Simulations. *J. Phys. Chem. B* **2015**, *119*, 13113−13133.

(42) Cuvier, A.-S.; Berton, J.; Stevens, C. V.; Fadda, G. C.; Babonneau, F.; Van Bogaert, I. N. A.; Soetaert, W.; Péhau-Arnaudet, G.; Baccile, N. pH-triggered formation of nanoribbons from yeast derived glycolipid biosurfactants. *Soft Matter* **2014**, *10*, 3950−3959.

(43) Cuvier, A.-S.; Babonneau, F.; Berton, J.; Stevens, C. V.; Fadda, G. C.; Genois, I.; Le Griel, P.; Péhau-Arnaudet, G.; Baccile, N. Synthesis of Uniform, Monodisperse, Sophorolipid Twisted Ribbons. *Chem. - Asian J.* **2015**, *10*, 2419−2426.

(44) Ballauff, M.; Jusufi, A. Anomalous small-angle X-ray scattering: analyzing correlations and fluctuations in polyelectrolytes. *Colloid Polym. Sci.* **2006**, *284*, 1303−1311.

(45) Jusufi, A. Fluctuation effects and monomer-counterion correlations in starlike polyelectrolyte systems. *J. Chem. Phys.* **2006**, *124*, 044908.

(46) Nagarajan, R. Self-assembly of bola amphiphiles. *Chem. Eng. Commun.* **1987**, *55*, 251−273.

(47) Glatter, O.; Kratky, O. *Small Angle X-ray Scattering*; Academic Press: London, 1982.

(48) Teixeira, J. Small-Angle Scattering by Fractal Systems. *J. Appl. Crystallogr.* **1988**, *21*, 781−785.

(49) Max, J.-J.; Chapados, C. Infrared Spectroscopy of Aqueous Carboxylic Acids: Comparison between Different Acids and Their Salts. *J. Phys. Chem. A* **2004**, *108*, 3324−3337.

(50) Tait, M. J.; Suggett, A.; Franks, F.; Ablett, S.; Quickenden, P. A. Hydration of monosaccharides: A study by dielectric and nuclear magnetic relaxation. *J. Solution Chem.* **1972**, *1*, 131−151.

(51) Miyajima, K.; Sawada, M.; Nakagaki, M. Studies on Aqueous Solutions of Saccharides. II. Viscosity B-Coefficients, Apparent Molar Volumes, and Activity Coefficients of D-Glucose, Maltose, and Maltotriose in Aqueous Solutions. *Bull. Chem. Soc. Jpn.* **1983**, *56*, 1954−1957.

(52) Li, X.-J.; Schick, M. Theory of Tunable pH-Sensitive Vesicles of Anionic and Cationic Lipids or Anionic and Neutral Lipids. *Biophys. J.* **2001**, *80*, 1703−1711.

(53) Hafez, I. M.; Cullis, P. R. Cholesteryl hemisuccinate exhibits pH sensitive polymorphic phase behavior. *Biochim. Biophys. Acta, Biomembr.* **2000**, *1463*, 107−114.

(54) Hafez, I. M.; Ansell, S.; Cullis, P. R. Tunable pH sensitive liposomes composed of mixtures of cationic and anionic lipids. *Biophys. J.* **2000**, *79*, 1438−1446.

(55) LeNeveu, D. M.; Rand, R. P.; Parsegian, V. A.; Gingell, D. Measurement and modification of forces between lecithin bilayers. *Biophys. J.* **1977**, *18*, 209−230.

(56) Rand, R. P.; Fuller, N.; Parsegian, V. A.; Rau, D. C. Variation in Hydration Forces between Neutral Phospholipid Bilayers: Evidence for Hydration Attraction. *Biochemistry* **1988**, *27*, 7711−7722.

(57) Di Gregorio, G. M.; Mariani, P. Rigidity and spontaneous curvature of lipidic monolayers in the presence of trehalose: a measurement in the DOPE inverted hexagonal phase. *Eur. Biophys. J.* **2005**, *34*, 67−81.

(58) Fromherz, P. Lipid-vesicle structure: size control by edge-active, agents. *Chem. Phys. Lett.* **1983**, *94*, 259−266.

(59) Madenci, D.; Salonen, A.; Schurtenberger, P.; Pedersen, J. S.; Egelhaaf, S. U. Simple model for the growth behaviour of mixed lecithin−bile salt micelles. *Phys. Chem. Chem. Phys.* **2011**, *13*, 3171−3178.

(60) Zemb, Th.; Dubois, M.; Deme, B.; Gulik-Krzywicki, Th. Self-assembly of flat nanodiscs in salt-free catanionic surfactant solutions. *Science* **1999**, *283*, 816.

(61) Carriere, D.; Belloni, L.; Deme, B.; Dubois, M.; Vautrin, C.; Meister, A.; Zemb, Th. In-plane distribution in mixtures of cationic and anionic surfactants. *Soft Matter* **2009**, *5*, 4983.

(62) Manohar, C.; Narayanan, J. Edge−edge attractions in surfactant nanodiscs: Implications. *Chem. Phys. Lett.* **2011**, *517*, 176−179.

(63) Nicolai, T.; Pouzot, M.; Durand, D.; Weijers, M.; Visschers, R. W. Iso-scattering points during heat-induced aggregation and gelation of globular proteins indicating micro-phase separation. *Europhys. Lett.* **2006**, *73*, 299−305.

(64) Chalal, M.; Ehrburger-Dolle, F.; Morfin, I.; Bley, F.; Aguilar de Armas, M.-R.; Lopez Donaire, M.-L.; San Roman, J.; Bolgen, N.; Piskin, E.; Ziane, O.; Casalegno, R. SAXS Investigation of the Effect of Temperature on the Multiscale Structure of a Macroporous Poly(N-isopropylacrylamide) Gel. *Macromolecules* **2010**, *43*, 2009−2017.

(65) Johnson, R. W. Diffraction Isosbestic Points And Structural Systematics In The Si$_x$Se$_{1-x}$ Glass System. *J. Non-Cryst. Solids* **1986**, *88*, 366−380.

(66) Walsh, D. M.; Lomakin, A.; Benedek, G. B.; Condron, M. M.; Teplow, D. B. Amyloid β-Protein Fibrillogenesis Detection Of A Protofibrillar Intermediate. *J. Biol. Chem.* **1997**, *272*, 22364−22372.

(67) Lomakin, A.; Chung, D. S.; Benedek, G. B.; Kirschner, D. A.; Teplow, D. B. On the nucleation and growth of amyloid, 8-protein fibrils: Detection of nuclei and quantitation of rate constants. *Proc. Natl. Acad. Sci. U. S. A.* **1996**, *93*, 1125−1129.

(68) Sabate, R.; Estelrich, J. Evidence of the Existence of Micelles in the Fibrillogenesis of â-Amyloid Peptide. *J. Phys. Chem. B* **2005**, *109*, 11027−11032.

(69) Martel, A.; Burghammer, M.; Davies, R. J.; Di Cola, E.; Vendrely, C.; Riekel, C. Silk Fiber Assembly Studied by Synchrotron Radiation SAXS/WAXS and Raman Spectroscopy. *J. Am. Chem. Soc.* **2008**, *130*, 17070−17074.

(70) Auer, S.; Dobson, C. M.; Vendruscolo, M. Characterization of the nucleation barriers for protein aggregation and amyloid formation. *HFSP J.* **2007**, *1*, 137−146.